

# Towards Full Automation of Geometry Extraction for Biomechanical Analysis of Abdominal Aortic Aneurysm; Neural Network-Based versus Classical Methodologies

Farah Alkhatib<sup>1</sup>, Mostafa Jamshidian<sup>1</sup>, Donatien Le Liepvre<sup>2</sup>, Florian Bernard<sup>2</sup>, Ludovic Minvielle<sup>2</sup>, Adam Wittek<sup>1</sup>, Karol Miller<sup>1,\*</sup>

<sup>1</sup> Intelligent Systems for Medicine Laboratory, The University of Western Australia, Perth, Western Australia, Australia

<sup>2</sup> Nurea, Bordeaux, France

## Abstract

In this study we investigated the impact of image segmentation methods on the results of stress computation in the wall of abdominal aortic aneurysms (AAAs). We compared wall stress distributions and magnitudes calculated from geometry models obtained from classical semi-automated segmentation versus automated neural network-based segmentation. Ten different AAA contrast-enhanced computed tomography (CT) images were semi-automatically segmented by an analyst, taking, depending on the quality of an image, between 15 and 40 minutes of human effort per patient. The same images were automatically segmented using PRAEVAorta<sup>®2</sup>, commercial software by NUREA (<https://www.nurea-soft.com/>), developed based on artificial intelligence (AI) algorithms, requiring only 1-2 minutes of computer time per patient. Aneurysm wall stress calculations performed using the BioPARR software (<https://bioparr.mech.uwa.edu.au/>) revealed that, compared to the classical semi-automated segmentation, the automatic neural network-based segmentation leads to equivalent stress distributions, and slightly higher peak and 99<sup>th</sup> percentile maximum principal stress values. This difference is due to consistently larger lumen surface areas in automatically segmented models as compared to classical semi-automated segmentations, resulting in greater total pressure load on the wall. Our findings are a steppingstone toward a fully automated pipeline for biomechanical analysis of AAAs, starting with CT scans and concluding with wall stress assessment, while at the same time highlighting the critical importance of the repeatable and accurate segmentation of the lumen, the difficult problem often underestimated by the literature.

---

\* Corresponding author.

E-mail address: [karol.miller@uwa.edu.au](mailto:karol.miller@uwa.edu.au) (K. Miller).

# 1 Introduction

Abdominal Aortic Aneurysm (AAA) disease is an asymptomatic condition, usually diagnosed accidentally through imaging indicated by some other health problem. While most AAAs never rupture or generate symptoms, those which rupture cause almost certain death (Wanhainen, Verzini et al. 2019, NICE 2020). Therefore, understanding of the risk of rapid disease progression and rupture in AAAs is crucial for appropriate AAA disease management. The current management primarily relies on a maximum aortic diameter threshold, set at 55 mm for men and 50 mm for women, guiding surgeons in their decision-making regarding the need for intervention (Wanhainen, Verzini et al. 2019). However, the recognized limitations of this approach become evident as most AAAs with a diameter larger than 55 mm remain stable throughout the patient's lifetime (Darling, Messina et al. 1977, Wanhainen, Verzini et al. 2019, NICE 2020).

This underscores the potential advantages that could arise from the use of biomechanical models to improve AAA disease progression and rupture risk assessment (Fillinger, Raghavan et al. 2002, Fillinger, Marra et al. 2003, Vande Geest, Di Martino et al. 2006, Gasser, Auer et al. 2010, Joldes, Miller et al. 2017, Miller, Mufty et al. 2020). Aortic wall stress has been the main variable of interest in almost all proposed biomechanical rupture risk indicators of AAA (Fillinger, Raghavan et al. 2002, Fillinger, Marra et al. 2003, Vande Geest, Di Martino et al. 2006, Gasser, Auer et al. 2010, Joldes, Miller et al. 2017). Computation of patient-specific aortic wall stress requires patient-specific geometry usually acquired through segmenting medical images.

The segmentation of AAA from medical images is a procedure that has historically taken a significant amount of an analyst time (Siriapisith, Kusakunniran et al. 2018). Manual segmentation of the aneurysm walls, which involves tracing the boundaries of the wall on each image slice, is a subjective process that can take very significant amount of time. Even semi-automatic segmentation methods using well-established intensity or intensity gradient-based classical algorithms require often as much as 45 minutes of work by a trained analyst per patient (Joldes, Miller et al. 2017). While it may be acceptable for research purposes, it is not practical for routine clinical use.

Artificial intelligence (AI)-based algorithms have emerged as promising tools for automatically segmenting aneurysms without user input (López-Linares, Aranjuelo et al. 2018, Lareyre, Adam et al. 2019, Caradu, Spampinato et al. 2021, Brutti, Fantazzini et al. 2022). A fully automated method for locating the aortic lumen and describing the AAA—including the identification of intraluminal thrombus (ILT) and calcifications—was introduced by (Lareyre, Adam et al. 2019). Tested on a cohort of 40 AAA patients utilizing computed tomography angiography (CTA) images, the methodology demonstrated a robust correlation with outcomes obtained from manual segmentation by an expert. A fully automated algorithm for segmenting ILT from CTA images and subsequent analysis of AAA geometry was recently proposed by (Brutti, Fantazzini et al. 2022). They implemented a deep-learning-based pipeline that uses CTA scans to localize and segment the thrombus. Eight CTA scans were used to validate this approach after it was trained on 63 CTA scans.

The accuracy and reproducibility of the segmentation are crucial for ensuring the validity of stress calculations in the AAA biomechanical analysis (Hodge, Tan et al. 2023). Our recent study (Hodge, Tan et al. 2023) revealed differences in the distribution of the calculated stress in the aneurysm wall between the segmentations done by different analysts. Notably, the differences in stress computed using geometries derived from classical and AI-based algorithm segmentations have yet to be analyzed.

In this study, we undertake a comparative aneurysm wall stress analysis of ten AAA geometries extracted through semi-automated segmentation by an analyst and a fully automated segmentation employing the AI algorithm developed by Nurea (<https://www.nurea-soft.com/>). The computed aneurysm wall stress from both sets of geometries is compared using peak and 99<sup>th</sup> percentile of maximum principal stress and overall stress distributions. We used the method embedded in the freely-available open-source software platform BioPARR – Biomechanics-based Prediction of Aneurysm Rupture Risk (<https://bioparr.mech.uwa.edu.au/>) (Joldes, Miller et al. 2016, Joldes, Miller et al. 2017) to perform the stress calculations of the aneurysm wall.

## 2 Materials and Methods

### 2.1 Patient-Specific Abdominal Aortic Aneurysm (AAA) Geometries

In this study, we utilized anonymized contrast-enhanced CTA image data sets of ten AAA patients (Alkhatib, Wittek et al. 2023). Patients were recruited at Fiona Stanley Hospital (Western Australia, Australia) and provided their informed consent prior to their involvement in the research. The study was conducted in accordance with the Declaration of Helsinki, and the protocol was approved by Human Research Ethics and Governance at South Metropolitan Health Service (HREC-SMHS) (approval code RGS3501), and by Human Research Ethics Office at The University of Western Australia (approval code RA/4/20/5913). **Table 1** summarizes the medical image properties for each patient. The collected CTA images differed in size and resolution between individuals, contingent on the permitted radiation dose received by each patient which depends on patient's weight and height.

**Table 1** Computed tomography angiography (CTA) image dimensions and resolutions for the studied abdominal aortic aneurysm (AAA) patients; and the mean arterial blood pressure in kPa for all patients.

Patient no.	Image dimensions	Image spacing/ resolution (mm)	Mean arterial blood pressure (kPa)
1	512×512×1156	0.39×0.39×0.20	12
2	512×512×169	0.63×0.63×0.94	13
3	256×256×254	1.18×1.18×1.00	13
4	256×256×177	0.81×0.81×0.42	14
5	256×256×482	1.82×1.82×1.00	14
6	256×256×452	1.55×1.55×1.00	15
7	256×256×488	1.53×1.53×1.00	9
8	256×256×188	1.25×1.25×1.00	13
9	512×512×160	0.63×0.63×1.00	12
10	512×512×174	0.62×0.62×1.00	13

### 2.1.1 Semi-automatic intensity-based segmentation

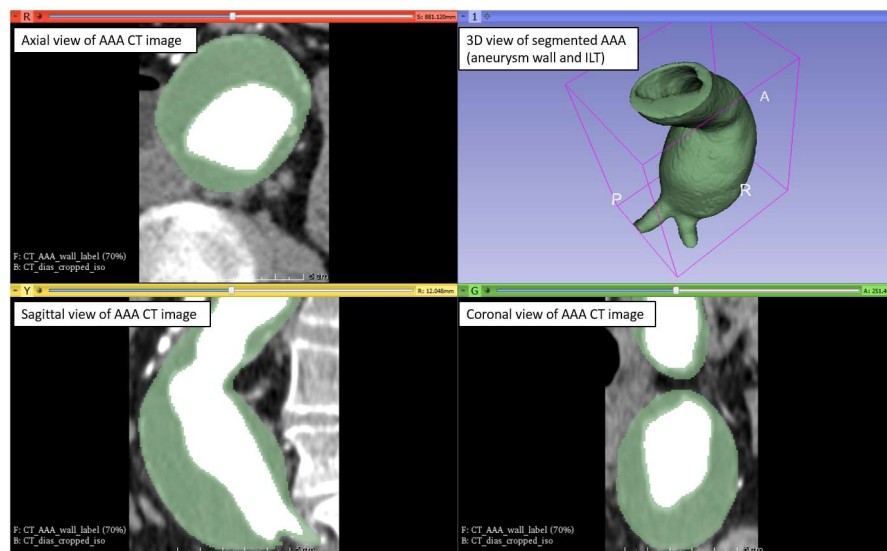
The classical semi-automated segmentation was carried out using 3D Slicer, an open-source software platform for medical images informatics, image processing, and three-dimensional visualization (<https://www.slicer.org/>) (Fedorov, Beichel et al. 2012). This classical segmentation approach has been employed in our previous studies (Joldes, Miller et al. 2017, Miller, Mufty et al. 2020, Alkhatib, Bourantas et al. 2023, Alkhatib, Wittek et al. 2023, Hodge, Tan et al. 2023). The CTA image was imported into 3D Slicer as DICOM (Digital Imaging and Communications in Medicine) file and cropped to designate the region of interest for the AAA, which was located distal to the renal arteries and proximal to the common iliac bifurcations.

We used the intensity threshold algorithm (Lesage, Angelini et al. 2009) available in 3D Slicer to automatically segment the lumen (**Figure 1a**). The threshold range was adjusted manually by an analyst for each patient's CT image. Any additional components detected by the threshold algorithm, aside from the aortic lumen, such as vertebrae, calcifications, and veins, were removed.

We used the "Grow from seeds" algorithm within 3D Slicer, which is an improved region-growing technique of the grow-cut algorithm described in (Zhu, Kolesov et al. 2014) to segment the aneurysm wall and the ILT (**Figure 1b**). Although it was efficient in reducing the amount of human input required, manual modifications using the paint sphere brush in 3D Slicer were still needed in some instances. Gaussian smoothing was applied to the AAA segmentations, using a standard deviation of the Gaussian kernel of 0.2. Depending on image quality, human effort required to produce required segmentation was between 15 and 40 minutes.



(a)



(b)

**Figure 1** Segmentation of abdominal aortic aneurysm (AAA) from computed tomography angiography (CTA) image using 3D Slicer software called from BioPARR (Joldes, Miller et al. 2017); **(a)** automated segmentation of the lumen using the threshold algorithm, and **(b)** semi-automated segmentation of the aneurysm wall and intraluminal thrombus (ILT).

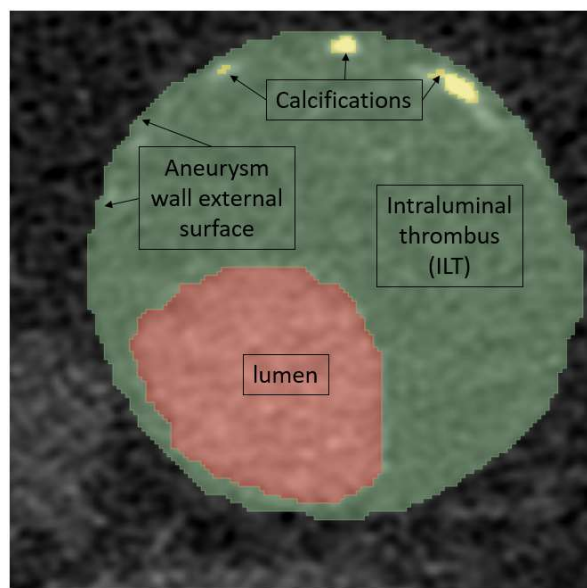
## 2.1.2 Fully automatic neural network-based segmentation

### 2.1.2.1 *Neural network segmentation*

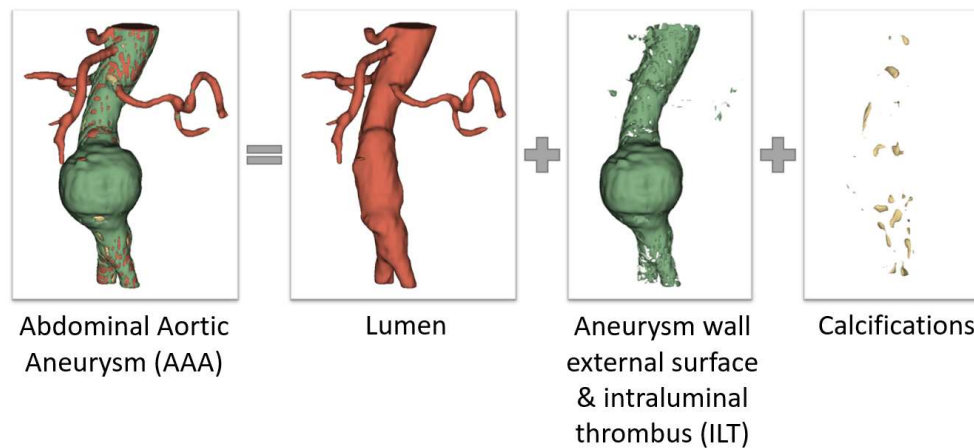
The fully automated segmentation was performed using PRAEVAorta<sup>®2</sup>, an automatic segmentation software developed by Nurea (<https://www.nurea-soft.com/>) that uses

convolutional neural networks similar to the classical Unet network (Bernard and Leguay 2021, Caradu, Spampinato et al. 2021, Caradu, Pouncey et al. 2022). This software is currently commercially available. The process of this AI-based segmentation consists of five sequential steps (Caradu, Spampinato et al. 2021, Caradu, Pouncey et al. 2022): (1) image pre-processing, to filter and denoise the medical images. (2) Localization of anatomical landmarks, to define the region of interest for the AAA. (3) Lumen segmentation using simple thresholding algorithm of the voxels in the region of interest. (4) Intraluminal thrombus segmentation that uses another algorithm to identify the surrounding tissue of the lumen and discriminate the aortic wall from the vena cava and the duodenum. (5) Thresholding based on pixel intensity (>500HU) to differentiate the calcifications from the thrombus (Bernard and Leguay 2021).

This fully automated AI segmentation algorithm uses DICOM CTA images to provide three labels: (i) aneurysm wall and ILT, (ii) calcification, and (iii) lumen segmentation. **Figure 2a** shows the axial view of the segmented AAA and **Figure 2b** shows the 3D rendered geometry from the same segmented AAA.



(a)



(b)

**Figure 2** The segmentation generated by the fully automated artificial intelligence (AI) segmentation algorithm (Caradu, Spampinato et al. 2021, Caradu, Pouncey et al. 2022) for the abdominal aortic aneurysm (AAA) consists of three labels: lumen is in red, aneurysm wall and intraluminal thrombus (ILT) are in green, and calcifications are in yellow colour. **(a)** An axial view of a computed tomography angiography (CTA) scan slice showing the segmentations, and **(b)** 3D geometries of AAA rendered from the segmentations.

#### 2.1.2.2 Post-processing of neural network segmentation

The immediate output of the AI-based segmentation could not be directly utilized in the BioPARR automatic pipeline for stress analysis because the AI-based segmentation algorithm did not detect the aneurysm wall in certain locations (**Figure 3**), resulting in voids, holes, and significant missing parts in the aneurysm wall. Furthermore, the lumen segmentation encompassed thin layers of the aneurysm external wall, which should have been part of the aneurysm wall and ILT segmentation. Therefore, we added, as a post-processing step, an automatic cleaning of AI-based segmentations using an in-house MATLAB code developed by the Intelligent Systems for Medicine Laboratory (ISML) at The University of Western Australia (UWA). The AI-based algorithm's segmentations were initially cropped by the region of interest employed in the semi-automated segmentation. The three labels (aneurysm wall and ILT, calcification and lumen) were merged to generate the AAA segmentation. Any additional branches of vessels or artefacts, other than the aorta, were removed to create the lumen segmentation. Both AAA and lumen segmentations were then resampled using nearest-neighbor interpolation to convert them into isotropic volumes, utilising the smallest dimension of the original anisotropic voxel size of the image. An initial



convolution smoothing was performed for each segmentation, specifically to eliminate thin-layer artefacts.

Convolution smoothing of a segmentation involves using convolution to blur the image and subsequently applying thresholding to obtain the smoothed segmentations. Convolution utilizes a kernel, represented as a matrix, that slides across the image and multiplies with the input to enhance the output in a desired manner, such as achieving smoothness in this context. In this process, a smoothing kernel is employed to effectively smooth both lumen and AAA segmentations and eliminate thin objects, addressing concerns like thin artefacts in the lumen segmentation. The cleaning process involves successive removal of extrusions, filling of holes, and smoothing each segmentation again. However, in one case (Patient 6 with a relatively large artifact extrusion) our cleaning process did not remove all artefacts in the segmentations. It nevertheless did not result in significant differences in the stress distribution, see **Section 3**. The cleaning process for both lumen and AAA segmentation is illustrated in **Figure 4**.

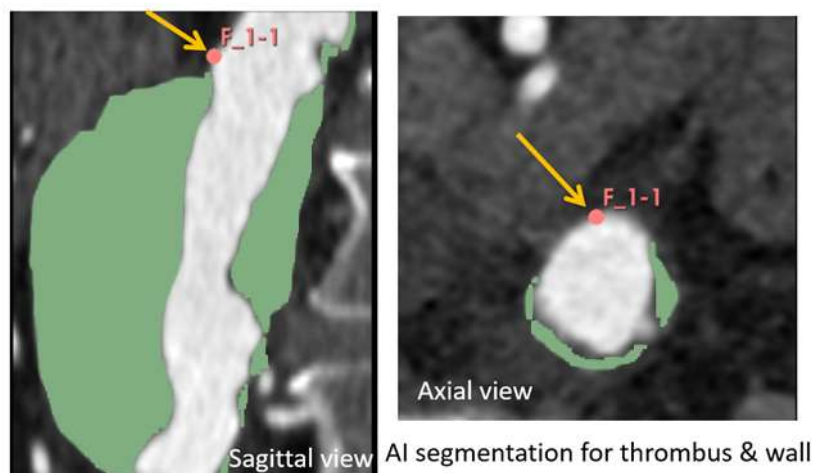


**Figure 3** The automatic segmentation by an artificial intelligence (AI) algorithm of the aneurysm wall and thrombus is in green color, and the fiducial point in both sagittal and axial views is the same point showing that the automatic algorithm could not detect the aneurysm wall in certain locations.

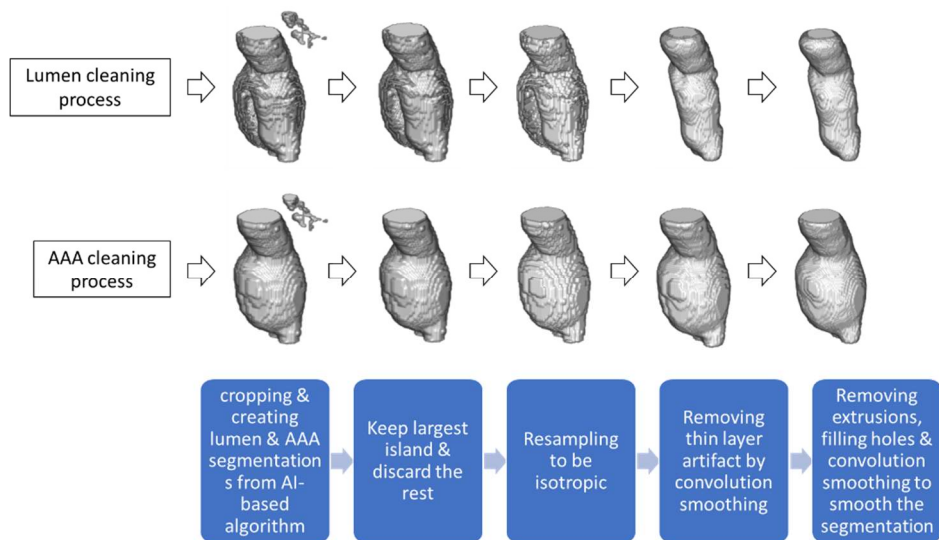


**Figure 4** The step-by-step post-process of the automatic artificial intelligence (AI)-based segmentation.

### 2.1.3 AAA geometries

Within the BioPARR software (Joldes, Miller et al. 2017), we utilized 3D Slicer to automatically define the surfaces of the aneurysm wall and the ILT using the created segmentations (**Figure 5**). A Laplacian smoothing was applied for all AAA geometries. A constant AAA wall thickness of 1.5 mm was assumed for the creation of patient-specific finite element meshes of AAA.

Since calcifications are typically not correlated with an increased risk of AAA rupture (Maier, Gee et al. 2010), they were not taken into consideration when developing the biomechanical models in this study. This is consistent with the AAA stress computation literature (Khosla, Morris et al. 2014, Gasser 2016, Gasser, Miller et al. 2022, Wittek, Alkhatib et al. 2022).

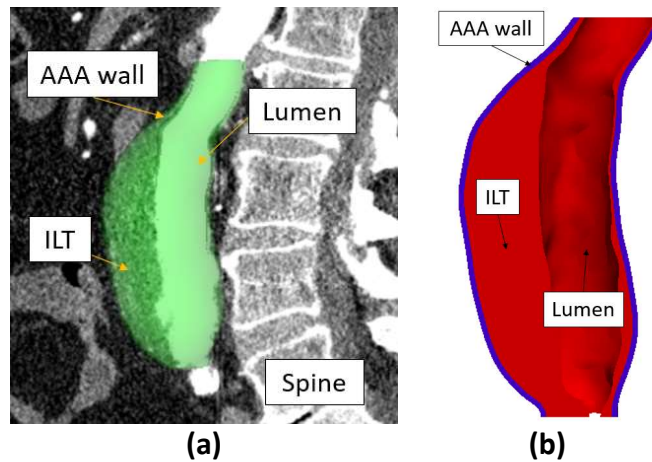


**Figure 5** Example of patient-specific abdominal aortic aneurysm (AAA) geometry (Patient 1): **(a)** AAA model segmented from computed tomography angiography (CTA) image - sagittal view, and **(b)** a cross-section of AAA geometry showing the intraluminal thrombus (ILT), lumen, and AAA external wall (blue color) created automatically using BioPARR (Joldes, Miller et al. 2017). Figure adapted from (Alkhatib, Wittek et al. 2023).

## 2.2 Stress Computation in Abdominal Aortic Aneurysm (AAA) Wall

To calculate the stress within the aneurysm wall, we used the method embedded in the freely-available open-source software platform BioPARR – Biomechanics-based Prediction of Aneurysm Rupture Risk (<https://bioparr.mech.uwa.edu.au/>) (Joldes, Miller et al. 2016, Joldes, Miller et al. 2017). The methods used in BioPARR have been described in detail elsewhere (Joldes, Miller et al. 2016, Joldes, Miller et al. 2017) and used previously in our papers (Wittek, Alkhatib et al. 2022, Alkhatib, Bourantas et al. 2023, Alkhatib, Wittek et al. 2023, Hodge, Tan et al. 2023). BioPARR calls Abaqus/Standard finite element code (Simulia 2024) for a linear static finite element analysis. The aneurysm stress is extracted from the known deformed geometry (as seen on CT) and pressure load using standard linear methods that are known to be insensitive to a stress parameter in the material constitutive law (Ciarlet 1988, Lu, Zhou et al. 2007, Zelaya, Goenezen et al. 2014, Biehler, Gee et al. 2015, Joldes, Miller et al. 2016, Joldes, Miller et al. 2017, Liu, Liang et al. 2019, Wittek, Alkhatib et al. 2022).

We incorporated the residual stresses according to Fung’s Uniform Stress Hypothesis (USH) (Fung 1991) by averaging the stress across the vessel wall thickness (Joldes, Noble et al. 2018). The residual stresses calculations are implemented within BioPARR platform (Joldes, Miller et al. 2016) as a simple post-processing step during the AAA biomechanical analysis.

### 2.2.1 Finite element meshes of AAA

The construction of computational grids (finite element meshes) for geometries extracted from the classical semi-automated segmentation and the automated AI-based segmentation followed the same process. Tetrahedral finite element meshes were automatically created from the AAA geometries using the open-source Gmsh mesh generator (Geuzaine and Remacle 2009, Geuzaine and Remacle 2024), called from within the BioPARR software (Joldes, Miller et al. 2017). Mesh optimization was employed during mesh generation to ensure the mesh quality. In line with our previous study (Alkhatib, Wittek et al. 2023), we determined that two quadratic tetrahedral elements through the wall thickness are sufficient for a converged solution in aneurysm wall stress calculation. For both the AAA arterial wall and the ILT, we utilized 10-noded tetrahedral elements with hybrid formulation to avoid volumetric locking (element type C3D10H in Abaqus finite element code).

### 2.2.2 Boundary conditions and load

The aneurysm's top and bottom nodes were rigidly constrained. The spine and tissues surrounding the aorta were not considered in the AAA computational biomechanics models created in this work. Such an approach is frequently used in the literature (Gasser, Auer et al. 2010, Joldes, Miller et al. 2016), and our recent study (Liddelow, Alkhatib et al. 2023) supports its applicability.

Patient-specific mean arterial blood pressure (MAP) (Cywinski 1980), measured ten minutes before the image acquisition, was used as patient-specific load. MAP ranged between 9 – 15 kPa with a median of 13 kPa (**Table 1**). The pressure load was uniformly distributed over the ILT luminal surface (Inzoli, Boschetti et al. 1993, Vorp, Mandarino et al. 1996).

### 2.2.3 Material models and material properties

A nearly incompressible linear elastic material model (Poisson's ratio = 0.49) for the aortic wall and ILT tissues was used. The aorta was defined as a very stiff material to ensure that the deformed geometry of AAA represented by the model remains unchanged when loaded by blood pressure (Joldes, Miller et al. 2016, Joldes, Miller et al. 2017, Miller, Mufty et

al. 2020, Wittek, Alkhatib et al. 2022). The ILT was assumed to be 20 times more compliant than the AAA wall (Miller, Mufty et al. 2020).

#### 2.2.4 Aneurysm wall stress comparison

In our analysis, we compared both the magnitude and distribution of the maximum principal stress calculated for AAA geometries extracted using the semi-automatic and automatic segmentations. We present the findings for the peak and 99<sup>th</sup> percentile of maximum principal stress in the aneurysm wall, as (Speelman, Bosboom et al. 2008) indicated that the 99<sup>th</sup> percentile of the aneurysm wall stress is more reproducible than the peak value of the maximum principal stress.

We generated maximum principal stress percentile plots for a quantitative assessment of aneurysm wall stress levels (Alkhatib, Wittek et al. 2023). On these plots, the horizontal axis represents the percentile rank of the maximum principal stress at a specific node within the entire population of nodes in the AAA finite element model for a given patient. The vertical axis corresponds to the actual value of the maximum principal stress at that node.

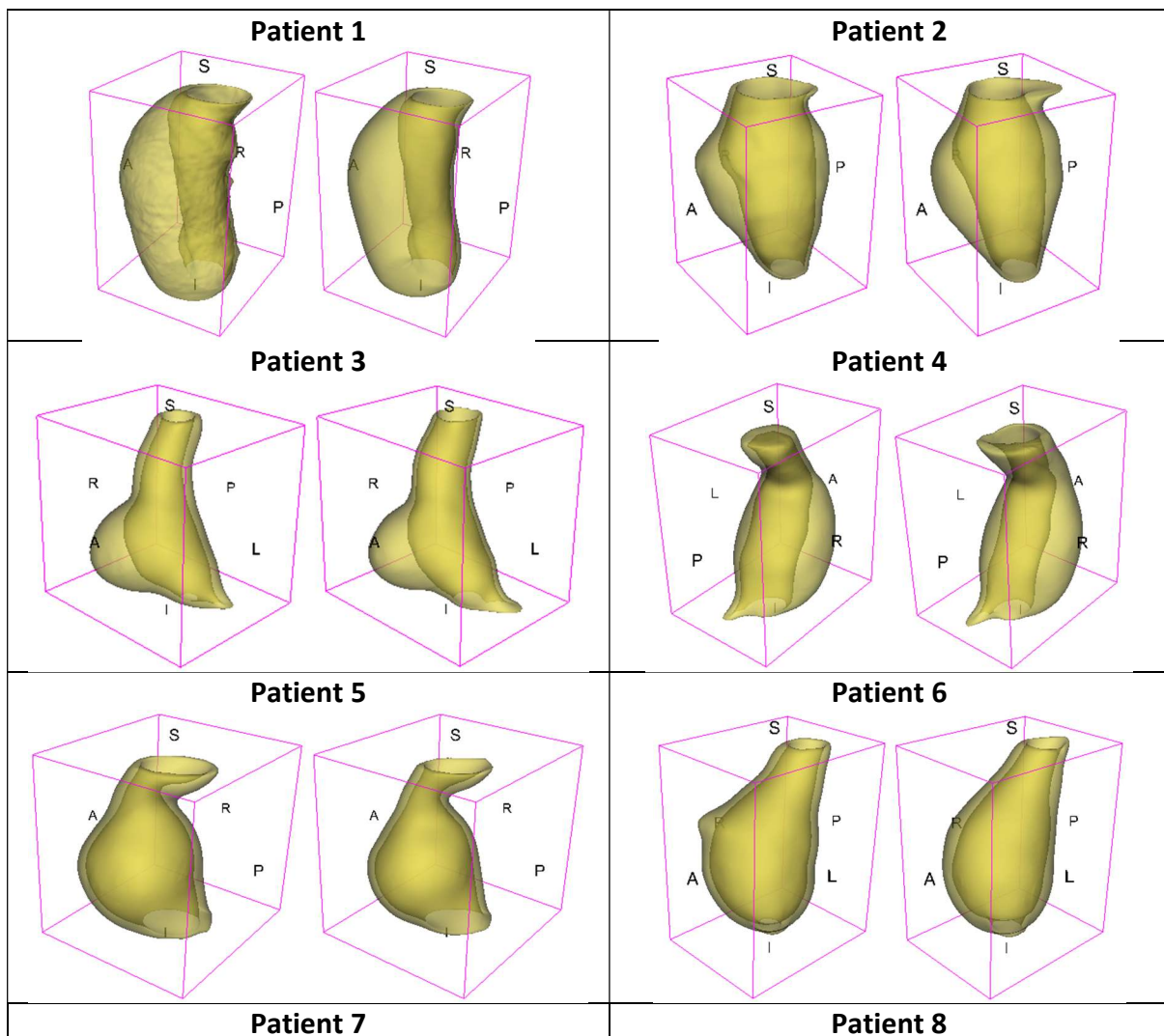
### 3 Results

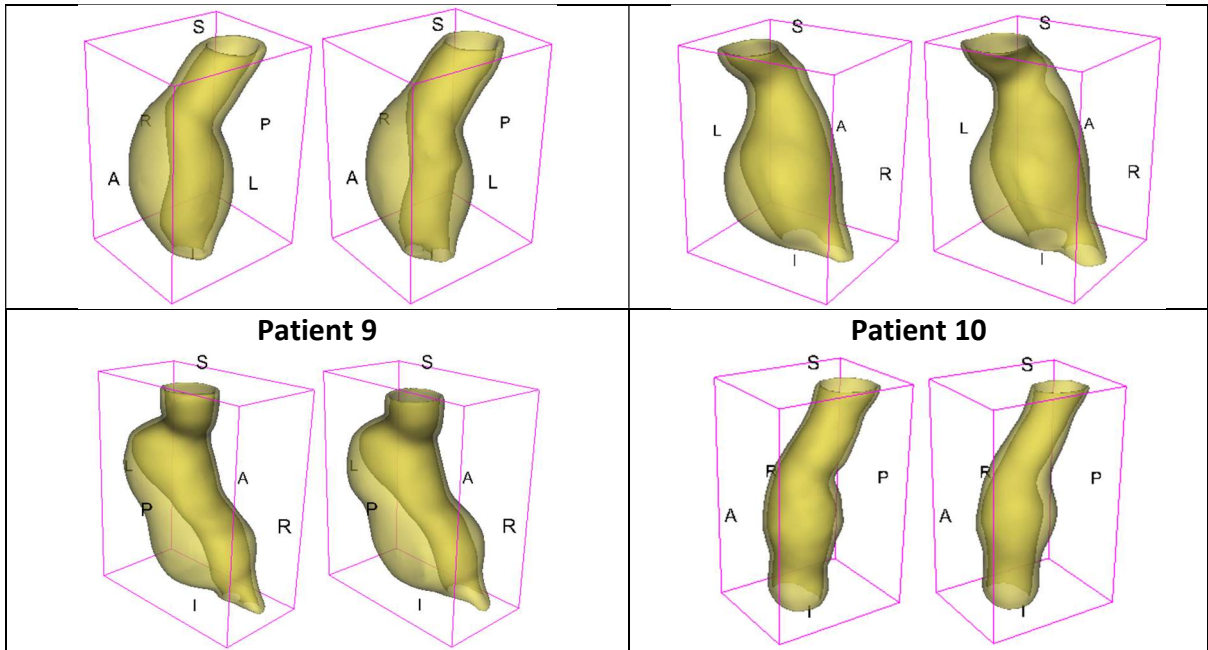
#### 3.1 Patient-specific Abdominal Aortic Aneurysm (AAA) Geometries

The classical semi-automated segmentation by an analyst took between 15 and 40 minutes of analyst time per patient using Intel(R) Core (TM) i7-8550U CPU @1.80 GHz with 16 GB of RAM running Windows 10 operating system. The automated segmentation using the AI algorithm took between 1 – 2 minutes of computer time per patient using a CPU Intel Xeon 8 cores 2.5GHz, 32 GB of RAM with a Tesla T4 GPU card. The subsequent automatic post-processing of the AI segmentation took a few seconds per patient using Intel(R) Core (TM) i9-12900H 2.50 GHz with 64 GB of RAM running Windows 10 operating system.

The automatic generation of the aneurysm wall geometry using 3D Slicer called from within BioPARR, took less than 30 seconds per patient using Intel(R) Core (TM) i7-5930K CPU @3.50 GHz with 64 GB of RAM running Windows 8 operating system. **Figure 6** compares the final output of the aneurysm wall geometries from both segmentation methods.

**Table 2** presents 3D rendered geometries of the segmented lumen and aneurysm wall for each patient generated through the automated AI-based algorithm. The geometries depict the results before and after post-processing. Although AI segmentations underwent a fully automated cleaning process, we noticed that it is possible for the automatic AI-based segmentation to introduce artefacts such as relatively large additional segment on the outer wall of the aneurysm, as seen in Patient 6 (**Figure 6**). Such an artefact could not be corrected by the post-process cleaning and needs to be addressed by the initial AI-based segmentation. Interestingly, the presence of this artefact did not significantly influence the computed stress distribution, see **Figure 7**.

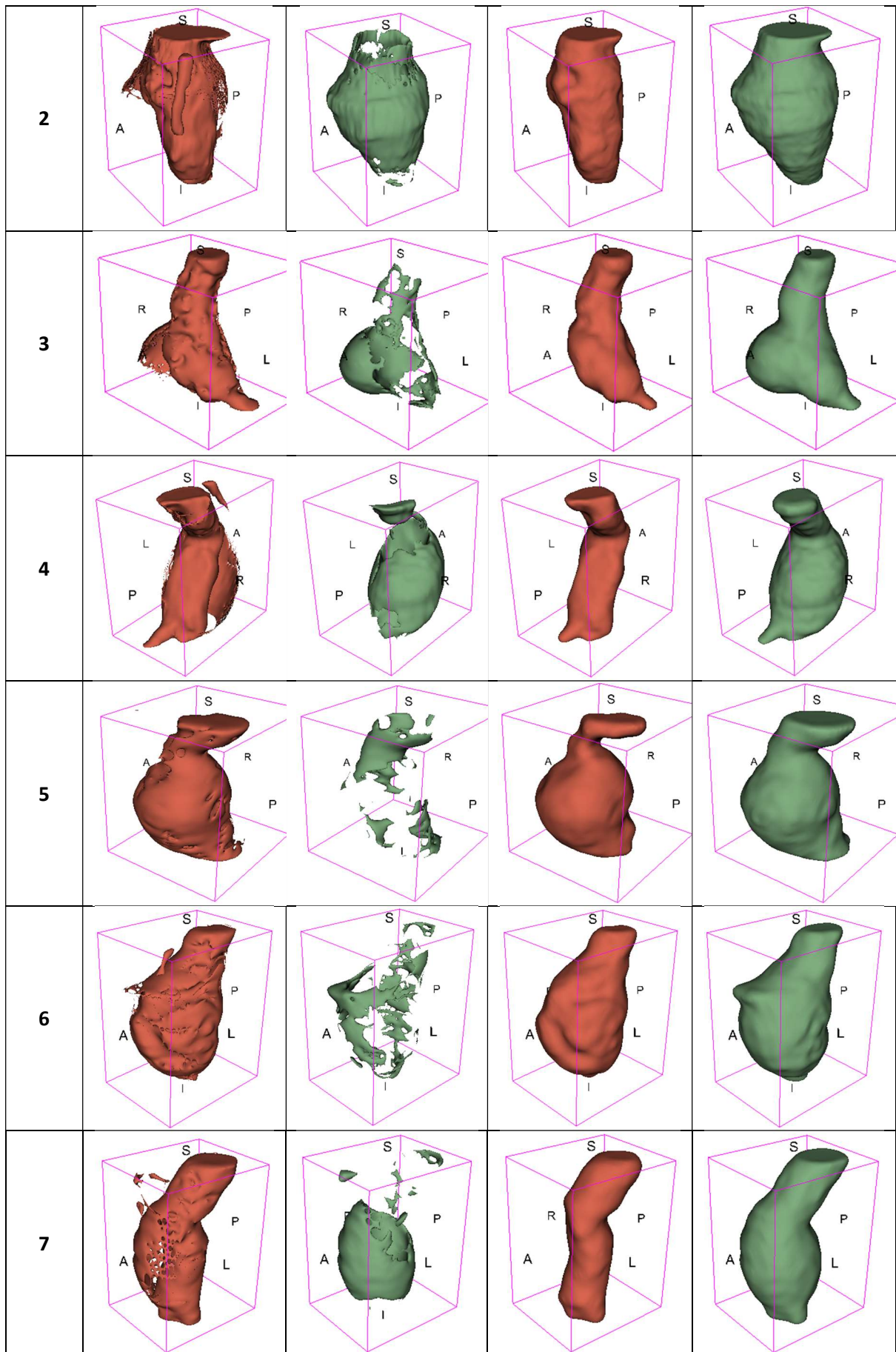




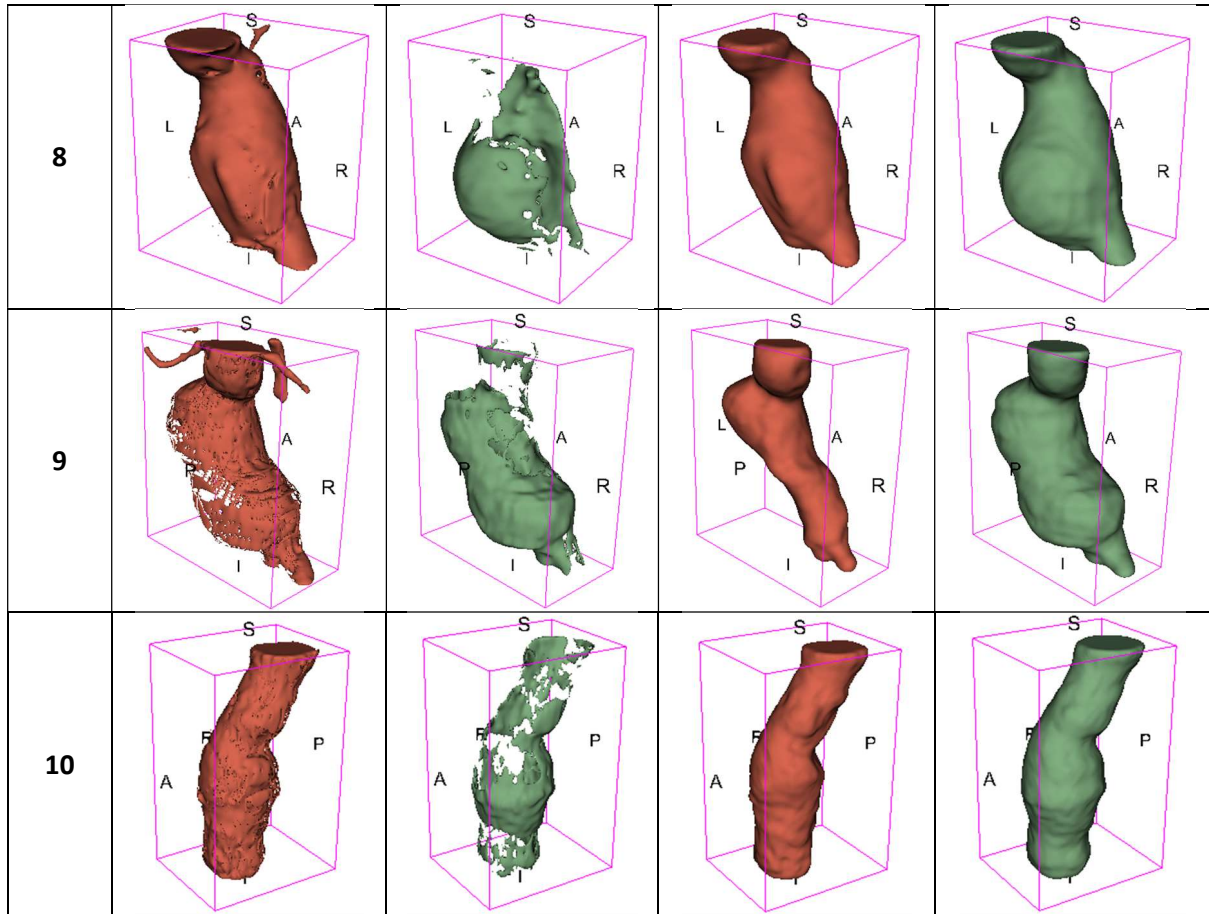
**Figure 6** Comparison of the aneurysm wall geometries created from the classical semi-automated segmentation by an analyst and the automatic segmentation using an artificial intelligence (AI) algorithm. The left-hand-side geometry is created from the automatic segmentation and the right-hand-side geometry is created from the semi-automated segmentation.

**Table 2** 3D rendered geometries of the lumen and abdominal aortic aneurysm (AAA) wall and intraluminal thrombus (ILT) created automatically by segmenting the computed tomography angiograph (CTA) images using an artificial intelligence (AI) algorithm showing the direct output from the algorithm and the output after applying a post-process step.

Patient no.	Raw segmentations created by the AI-based algorithm without any post-process cleaning		Segmentations created by the AI-based algorithm after the post-process cleaning	
	Lumen	AAA (Aneurysm wall & ILT)	Lumen	AAA (Aneurysm wall & ILT)
1				







### 3.2 Finite Element Meshes of Abdominal Aortic Aneurysm (AAA)

The automated tetrahedral mesh generation with optimization (Alkhatib, Wittek et al. 2023) took between 40 – 50 minutes per patient (aneurysm wall mesh generation and ILT mesh generation) using Intel(R) Core (TM) i7-5930K CPU@3.50 GHz with 64GB of RAM running Windows 8 operating system. The number of tetrahedral elements in the aneurysm wall varied between around 520,000 – 920,000 elements depending on the patient-specific aneurysm (**Table 3**), and the number of nodes varied between 820,000 and 1,400,000. The relative difference (**Equation 1**) in the number of elements between the aneurysm walls generated by the semi-automatic segmentation and the automatic segmentation ranged between -13% and +15% (**Table 3**), while the element count for the ILT exhibits significant variability, with relative differences between -54% and +67%, particularly evident in Patient 10 (**Table 3**).

$$\text{Relative difference} = \frac{v_{auto} - v_{semi}}{v_{semi}} \times 100\% \quad (1)$$

where  $v_{semi}$  is the variable of interest (i.e., number of nodes or number of elements in the patient-specific finite element mesh of AAA) from the semi-automatic segmentation and  $v_{auto}$  is the variable of interest from the automatic segmentation.

This variability in total number of elements is due to differences in smoothness of surfaces, whose triangulations initiated automatic tetrahedral meshing. Based on our experience, the AAA mesh refinement is sufficient to guarantee converged mesh-independent stress results (Alkhatib, Wittek et al. 2023).

**Table 3** Number of high-quality tetrahedral elements automatically constructed using Gmsh (Geuzaine and Remacle 2009, Geuzaine and Remacle 2024) called from within BioPARR (Joldes, Miller et al. 2017) for the abdominal aortic aneurysm (AAA) geometries extracted using semi-automatic segmentation and automatic artificial intelligence (AI)-based segmentation. Relative difference is calculated using **Equation 1**. ILT is intraluminal thrombus. Segmentation methods: Classical method is the semi-automated segmentation, and AI method is the automatic segmentation based on artificial intelligence (AI) algorithm.

Patient no.	Segmentation method	Wall	Relative difference (%)	ILT	Relative difference (%)	AAA (Wall + ILT)	Relative difference (%)
1	Classical	718,738	+5.8%	537,916	+17.9%	1,256,660	+11.0%
	AI	760,429		634,164		1,394,593	
2	Classical	849,479	+4.4%	665,981	+28.6%	1,515,464	+15.0%
	AI	886,653		856,509		1,743,162	
3	Classical	662,876	-13.8%	755,740	-54.6%	1,418,630	-35.5%
	AI	571,111		343,292		914,403	
4	Classical	855,299	-3.3%	470,965	+16.2%	1,326,267	+3.6%
	AI	826,671		547,120		1,373,791	
5	Classical	527,213	+13.4%	448,733	-4.3%	975,959	+5.2%
	AI	597,600		429,309		1,026,909	
6	Classical	624,894	-0.8%	433,014	-3.5%	1,057,909	-1.9%
	AI	619,726		417,873		1,037,599	
7	Classical	656,219	-10.6%	524,245	-31.6%	1,180,475	-19.9%
	AI	586,835		358,575		945,410	
8	Classical	863,937	-11.4%	810,900	-36.0%	1,674,848	-23.3%
	AI	765,167		518,620		1,283,787	
9	Classical	745,591	-1.7%	690,722	+13.7%	1,436,315	+5.7%
	AI	733,280		785,059		1,518,339	
10	Classical	796,538	+14.9%	658,838	+67.3%	1,455,391	+38.6%
	AI	915,373		1,102,296		2,017,669	

### 3.3 Aneurysm Wall Stress Analysis

Here we compare the peak values, 99<sup>th</sup> percentile and distribution of the maximum principal stress in the AAA wall obtained from models developed using semi-automated and automated AI-based segmentations. The comparison was conducted for all ten patients analyzed in this study.

The peak value of maximum principal stress (**Table 4**) was higher for eight aneurysm walls extracted using the automatic segmentation, however patients 3 and 9 showed higher peak of maximum principal stress in the semi-automatically segmented aneurysm wall compared to the automatically segmented walls. The 99<sup>th</sup> percentile maximum principal stress followed the same behavior as the peak maximum principal stress (**Table 4**).

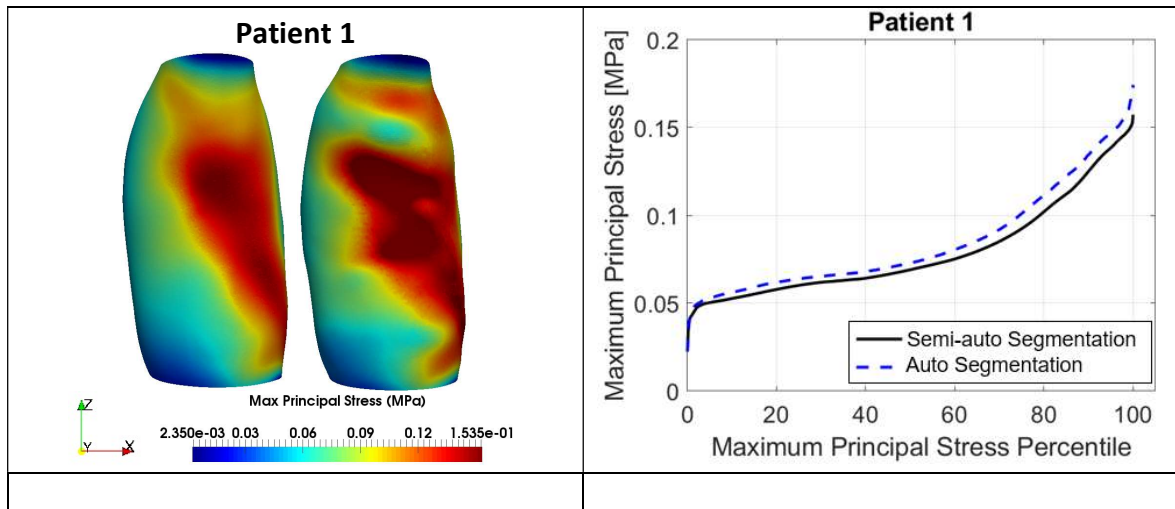
When analyzing the relative absolute difference in the peak of maximum principal stress, we noted the highest percentages for Patient 2 and Patient 10, reaching 22.8% and 37%, respectively (**Table 4**). To further investigate, we performed a stress analysis excluding the ILT from the finite element models, instead loading the inner surface of the aneurysm wall. The subsequent observation revealed a reduction in the relative absolute difference to 11.1% for Patient 2 and 8% for Patient 10. This implies a significant influence of the ILT segmentation on the stress analysis.

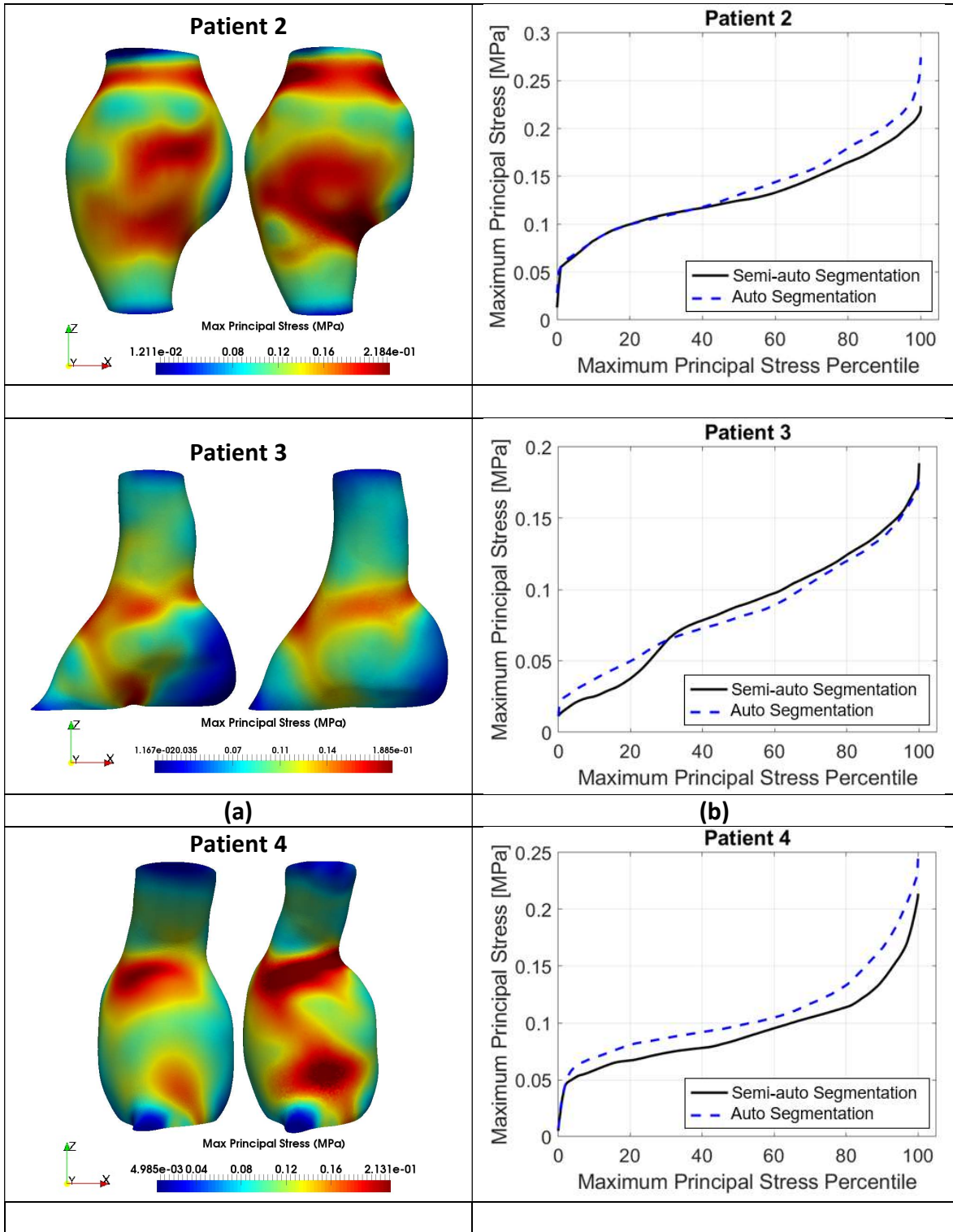
Contour plots of the maximum principal stress for the analyzed patients are shown in **Figure 7a**. Distributions of the percentile plots of the maximum principal stress in the aneurysm walls computed using the geometries extracted by the semi-automatic and automatic segmentations were very similar for all ten patients (**Figure 7b**), strongly suggesting that fully automatic segmentations can serve as the input compatible with clinical workflows for AAA stress analysis pipelines.

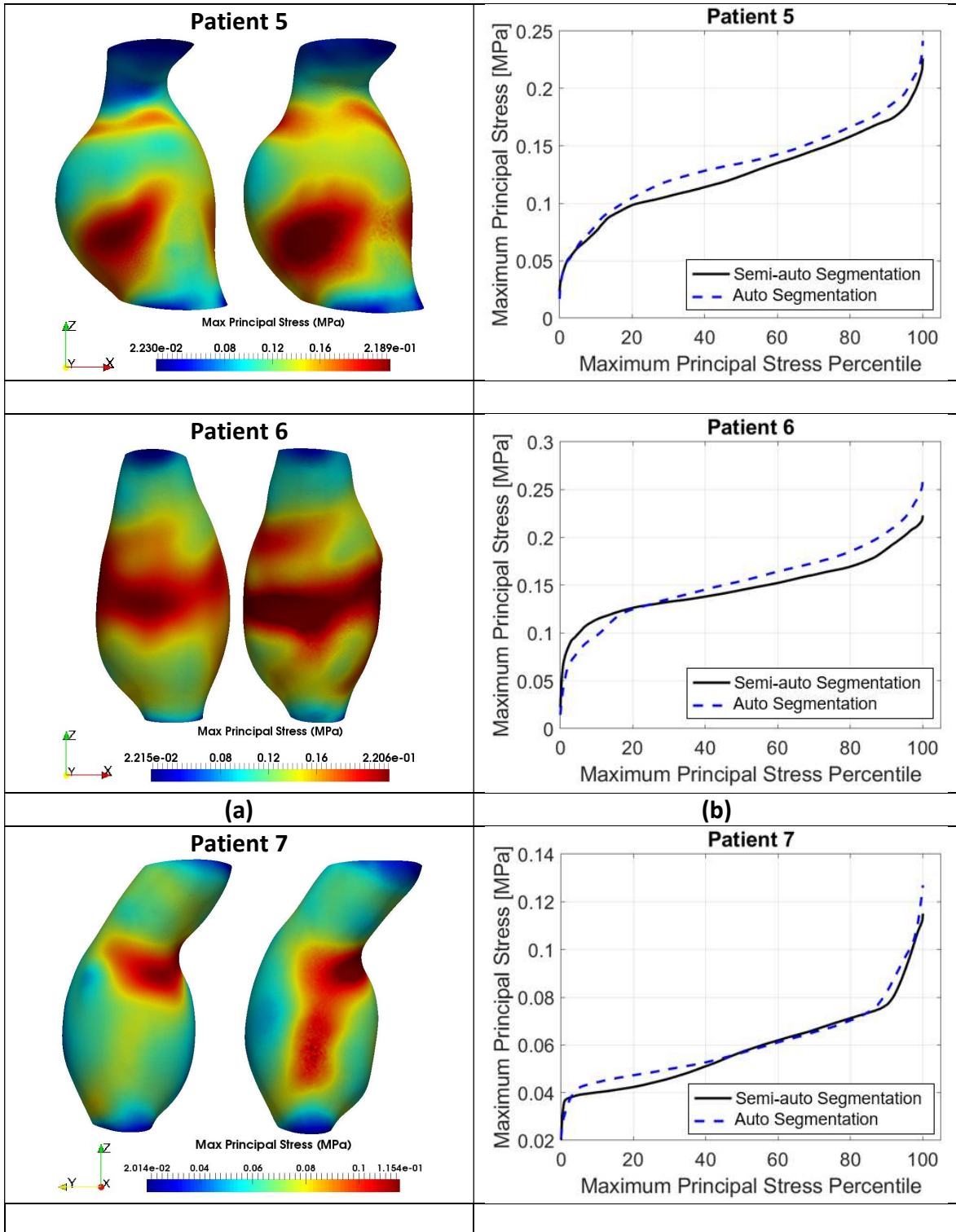
**Table 4** Comparison of peak and 99<sup>th</sup> percentile maximum principal stress, along with relative differences (calculated using **Equation 1**), between finite element models derived from semi-automated and automatic segmentations of abdominal aortic aneurysms (AAA). Segmentation methods: Classical method is the semi-automated segmentation, and AI method is the automatic segmentation based on artificial intelligence (AI) algorithm.

Patient no.	Segmentation method	Peak of maximum principal stress (MPa)	99 <sup>th</sup> percentile maximum principal stress (MPa)
-------------	---------------------	--	--

		Value	Relative difference %	Value	Relative difference %
1	Classical	0.1574	+11.0	0.1486	+7.8
	AI	0.1747		0.1602	
2	Classical	0.2237	+22.8	0.2117	+15.0
	AI	0.2748		0.2435	
3	Classical	0.1888	-5.5	0.1701	-1.4
	AI	0.1785		0.1678	
4	Classical	0.2141	+17.0	0.1959	+14.0
	AI	0.2505		0.2233	
5	Classical	0.2265	+7.6	0.2073	+5.8
	AI	0.2438		0.2194	
6	Classical	0.2229	+18.8	0.2141	+14.3
	AI	0.2648		0.2448	
7	Classical	0.1154	+10.1	0.1089	+5.6
	AI	0.127		0.1150	
8	Classical	0.2145	+3.6	0.2013	+2.1
	AI	0.2223		0.2056	
9	Classical	0.2087	-9.5	0.1913	-12.6
	AI	0.1888		0.1672	
10	Classical	0.1940	+37.0	0.1716	+28.3
	AI	0.2658		0.2201	







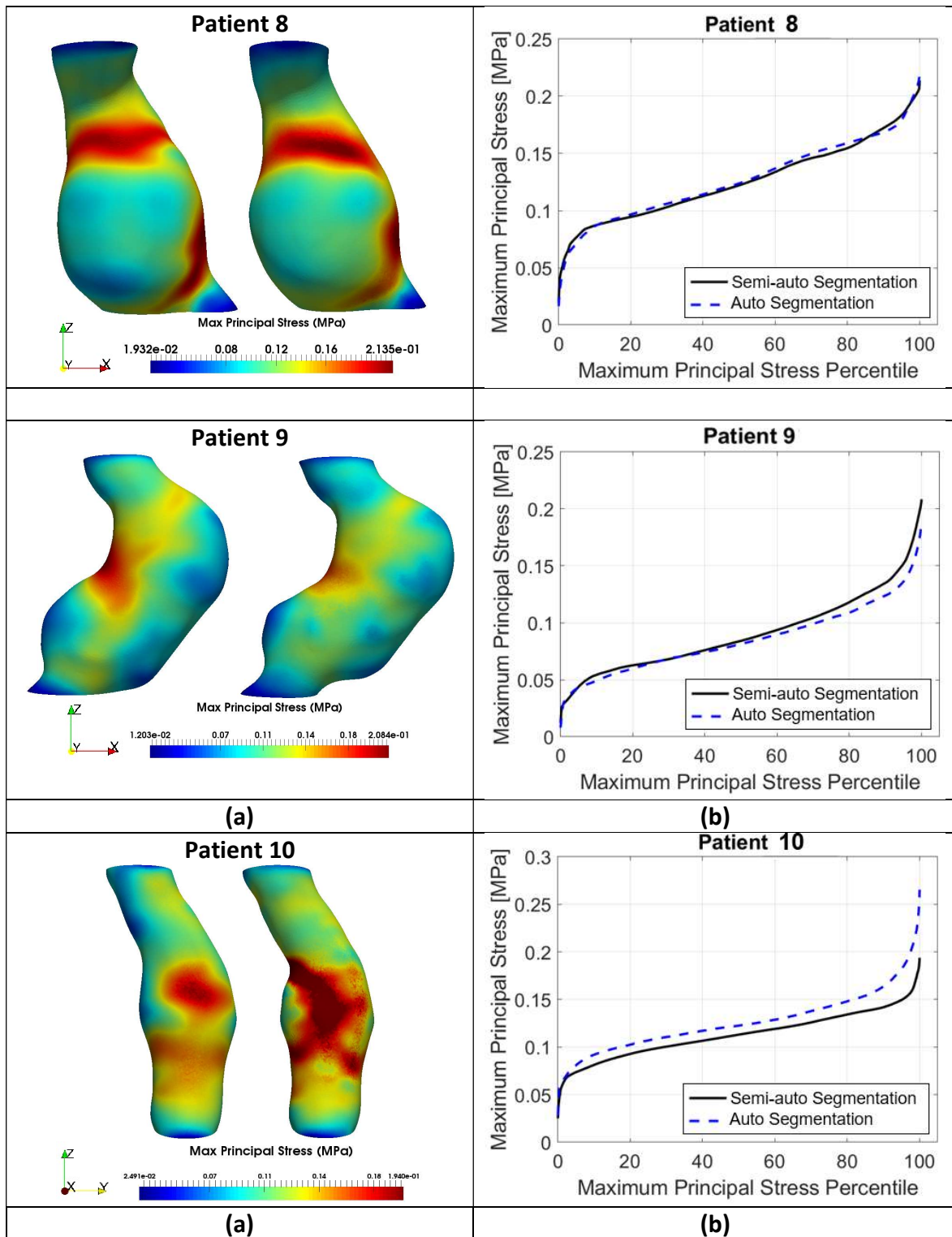


**Figure 7** Patient-specific finite element models of abdominal aortic aneurysm (AAA). **(a)** Contour plots of the maximum principal stress including residual stress in the aneurysm wall (Joldes, Noble et al. 2018) obtained using AAA geometries segmented semi-automatically (left-hand-side figures) and AAA geometries segmented automatically using artificial intelligence (AI) algorithm (right-hand-side figures); and **(b)** percentile plots of maximum principal stress for the studied AAA patients.

## 4 Discussion

The stress distributions on AAA walls and their values as seen on percentile plots, Figure 7, are very similar regardless of whether a fully automated AI-based or semi-automatic classical segmentation methodology was used. Nevertheless, in eight out of ten cases, the maximum and 99 percentile maximum principal stress values obtained from AAA finite element models using geometries extracted using AI-based automatic segmentation are higher than those based on semi-automatic segmentation.

As we have previously explored the impact of the finite element mesh on stress results (Alkhatib, Bourantas et al. 2023, Alkhatib, Wittek et al. 2023), we are certain that our computed stresses are mesh independent. This difference in maximum values of principal stress is due to variations in lumen segmentations. For eight out of ten cases, AI-based segmentation generated larger lumens than classical semi-automatic segmentations, and consequently larger surfaces on which pressure loads were applied in the finite element models, as discussed in more detail below.

### 4.1 Geometry and mesh

When comparing the number of elements in the ILT (**Table 3**), a notable difference emerged between semi-automated and automatic segmentations across most patients. Eight patients exhibited a relative absolute difference in the number of elements exceeding 10%. This difference is caused by slightly different smoothness of AAA wall surfaces, whose triangulations are used for initialization of automatic meshing. Our meshing method utilized the locations of nodes on the internal surface of the aneurysm wall as input for the external surface of the ILT, ensuring that surface nodes were shared and therefore that discretizations of the AAA wall and ILT were compatible (Alkhatib, Wittek et al. 2023).

The AI-based automatic segmentation generated a larger luminal surface compared to the luminal surface produced by the classical semi-automated segmentation (**Figure 8**). As the lumen surface is used to apply uniform pressure as loading in the finite element model, the differences in luminal surface areas directly translate to total loads and consequently to



computed stress magnitudes. Consequently, in eight out of ten cases, higher values for the maximum principal stress were observed in finite element models extracted through the fully automated segmentation compared to their semi-automatically segmented counterparts.

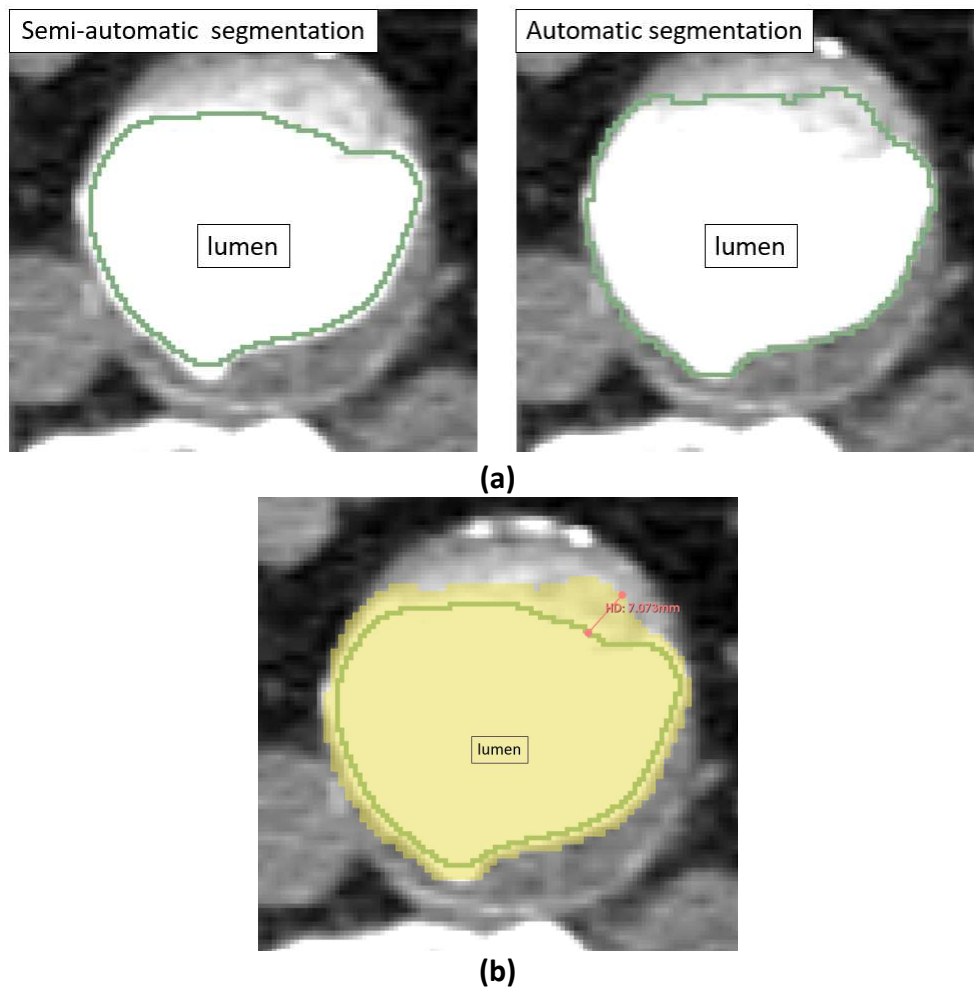


**Figure 8** Axial view of a slice from the computed tomography angiography (CTA) for an abdominal aortic aneurysm (AAA) (Patient 9) showing the lumen boundaries extracted using the threshold algorithm by semi-automatic segmentation where the threshold range was selected by an analyst and an automated segmentation where the threshold value was selected by an artificial intelligence (AI) algorithm. **(a)** Boundaries of the lumen are in green, and **(b)** the overlap of the two segmentations; yellow is the segmentation from the automatic segmentation and green boundary is the segmentation from the semi-automatic segmentation.

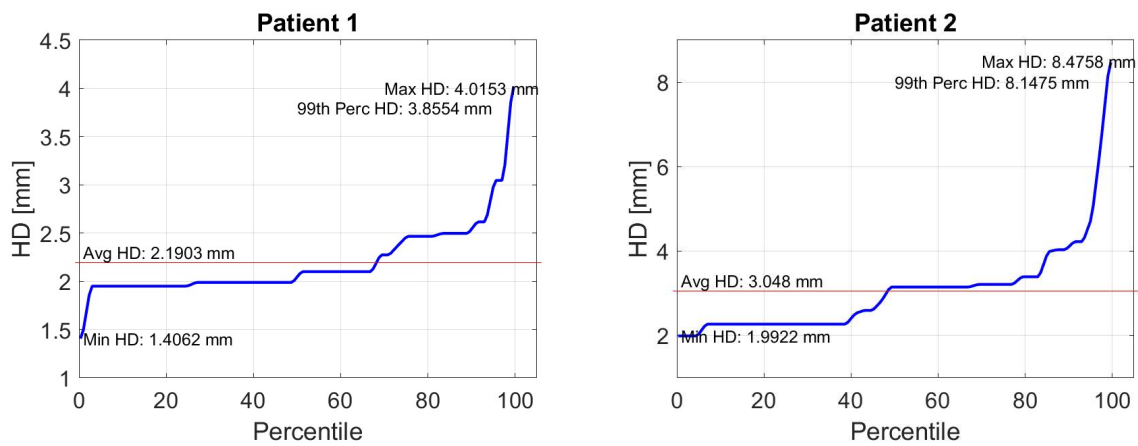
## 4.2 Lumen Segmentations Comparison

Due to uneven mixing of the contrast agent, determining the accurate lumen boundaries posed a challenge. In the absence of reliable ground truth, the question whether the semi-automatic or AI-based segmentation is “more correct” is difficult to answer. To gain additional insights into this important matter, we further expanded our investigation and calculated the Hausdorff distance (HD) (Rucklidge 1996, Garlapati, Mostayed et al. 2015) between the boundaries of the lumen segmented with both methods. HD was computed using the in-house MATLAB codes developed by the ISML team (Garlapati, Roy et al. 2014, Garlapati, Mostayed et al. 2015, Li, Miller et al. 2015). HD (**Equation 2**) is the maximum distance between the boundaries of the lumen segmentations.

$$HD(X, Y) = \max (h(X, Y), h(Y, X)) , \quad (2)$$

where X and Y represent the different segmentations

**Figure 9** shows the percentile plots of calculated Hausdorff distances within each slice of segmentation 2D axial view for the entire population of lumen boundaries segmented using both semi-automated and AI-based algorithm segmentations.



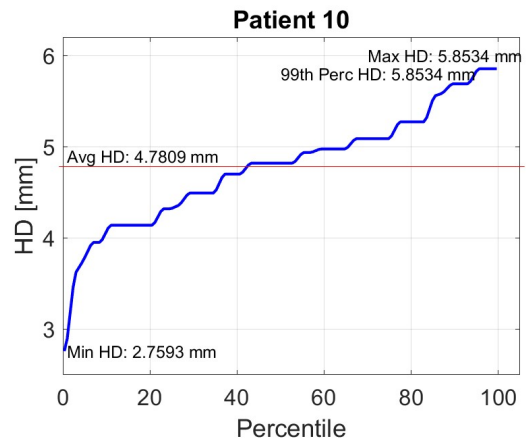
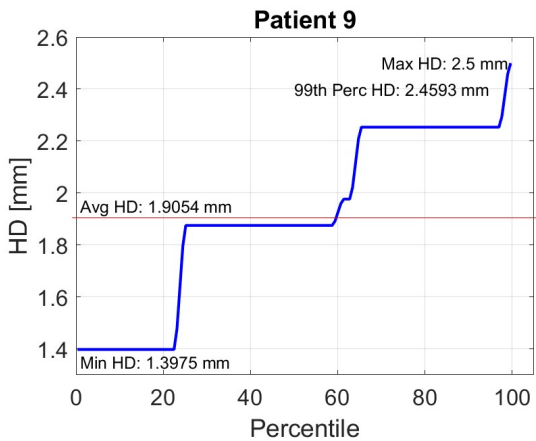
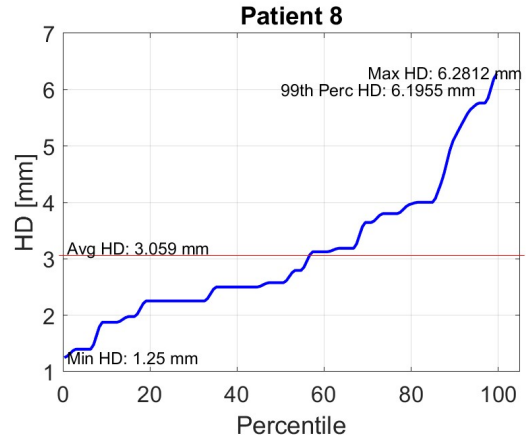
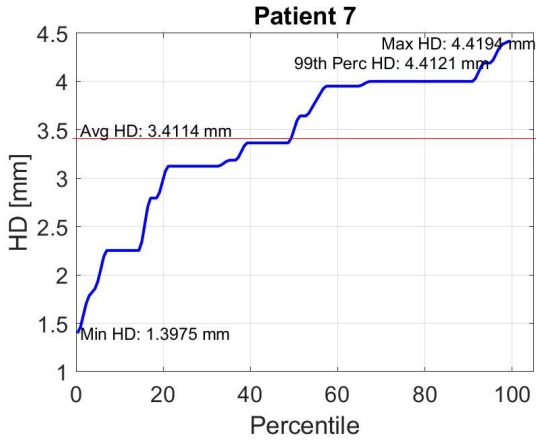
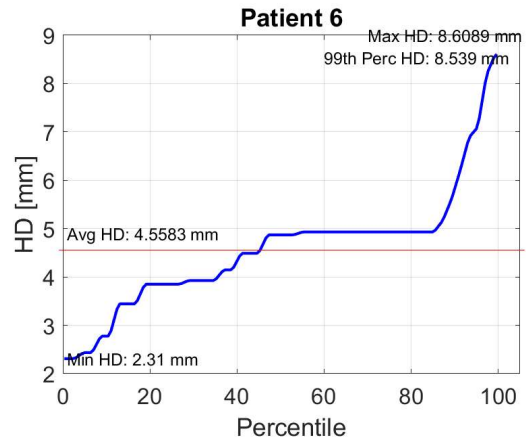
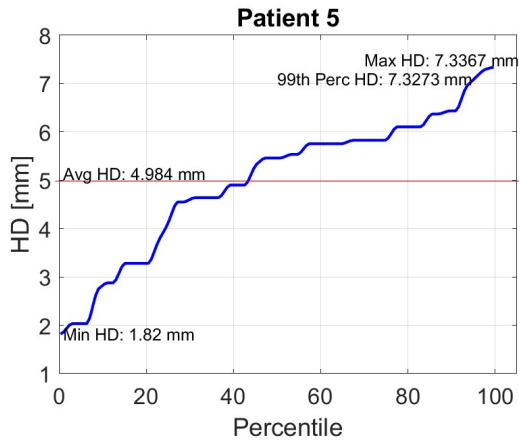
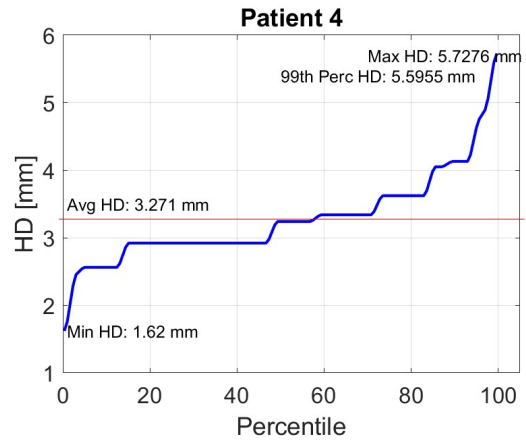
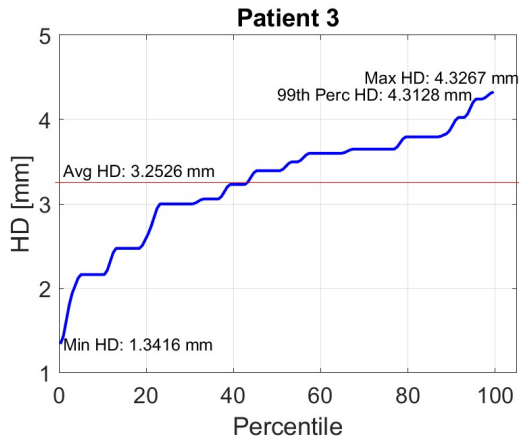


**Figure 9** Hausdorff Distance (HD) in mm between the segmented lumen boundaries in both segmentation methods, semi-automatic and automatic segmentations, against the percentile of edges in the axial image slices. The red dashed line indicates the average value of the HD distance.

As can be seen, the distances between contours are not insignificant, but while larger lumens of AI-segmented AAAs lead to slightly higher maximum principal stresses, fortunately they do not lead to different stress distribution patterns.

## 5 Conclusions

The findings of this study demonstrate a good correspondence between the stress calculations for abdominal aortic aneurysms (AAA) geometries extracted using a classical semi-automated segmentation and those generated through a fully automated segmentation employing an artificial intelligence (AI) algorithm. The peak and 99<sup>th</sup> percentile of maximum principal stress exhibited slightly higher values in the finite element models extracted through automatic segmentation compared to semi-automatic segmentation, while the distribution of maximum principal stress remained nearly identical.

This consistent difference in calculated maximum stress values was attributed to the AI algorithm's segmented lumens consistently exhibiting a larger surface area compared to semi-automatically segmented ones, resulting in larger total pressure load on the finite element model of AAA. This difference points to the importance of determining the lumen boundaries, a problem whose difficulty most probably stems from uneven mixing of a contrast agent used during imaging, and that is frequently underestimated in the literature. It also points to the need to rely on some normalized measure of stress, perhaps scaled by an “average stress”, rather than maximum (or 99 percentile) values.

In conclusion, our findings affirm the feasibility and reliability of a fully automated pipeline for stress evaluations in the context of abdominal aortic aneurysms, starting from patients' CT scans to aneurysm wall stress computations.

## Acknowledgment

This work was supported by the Australian National Health and Medical Research Council NHMRC Ideas grant no. APP2001689.

## 6 References

Alkhatib, F., G. C. Bourantas, A. Wittek and K. Miller (2023). Generation of Patient-specific Structured Hexahedral Mesh of Aortic Aneurysm Wall. Computational Biomechanics for Medicine - Towards Automation and Robustness of Computations in the Clinic. M. P. Nash, A. Wittek, P. M. F. Nielsen et al. Singapore, Springer International Publishing.

Alkhatib, F., A. Wittek, B. F. Zwick, G. C. Bourantas and K. Miller (2023). "Computation for Biomechanical Analysis of Aortic Aneurysms: The Importance of Computational Grid." Computer Methods in Biomechanics and Biomedical Engineering: 1-17.

Bernard, F. and R. Leguay (2021). Method for aiding in the diagnosis of a cardiovascular disease of a blood vessel (European Patent No. EP4264543A1). European Patent Office.

Biehler, J., M. W. Gee and W. A. Wall (2015). "Towards Efficient Uncertainty Quantification in Complex and Large-scale Biomechanical Problems Based on a Bayesian Multi-fidelity Scheme." Biomechanics and Modeling in Mechanobiology **14**(3): 489-513.

Brutti, F., A. Fantazzini, A. Finotello, L. O. Müller, F. Auricchio, B. Pane, G. Spinella and M. Conti (2022). "Deep Learning to Automatically Segment and Analyze Abdominal Aortic Aneurysm from Computed Tomography Angiography." Cardiovascular Engineering and Technology **13**(4): 535-547.

Caradu, C., A.-L. Pouncey, E. Lakhlifi, C. Brunet, X. Bérard and E. Ducasse (2022). "Fully Automatic Volume Segmentation using Deep Learning Approaches to Assess Aneurysmal Sac Evolution after Infrarenal Endovascular Aortic Repair." Journal of Vascular Surgery **76**(3): 620-630.e623.

Caradu, C. M. D., B. M. D. Spampinato, A. M. M. D. Vrancianu, X. M. D. P. Bérard and E. M. D. Ducasse (2021). "Fully Automatic Volume Segmentation of Infrarenal Abdominal Aortic Aneurysm Computed Tomography Images with Deep Learning Approaches versus Physician Controlled Manual Segmentation." Journal of Vascular Surgery **74**(1): 246-256.e246.

Ciarlet, P. G. (1988). Mathematical Elasticity, North Holland. The Netherlands.

Cywinski, J. (1980). The Essentials in Pressure Monitoring, Springer Dordrecht.

Darling, R., C. Messina, D. Brewster and L. Ottinger (1977). "Autopsy Study of Unoperated Abdominal Aortic Aneurysms. The Case for Early Resection." Circulation **56**(3 Suppl): II161-164.

Fedorov, A., R. Beichel, J. Kalpathy-Cramer, J. Finet, J.-C. Fillion-Robin, S. Pujol, C. Bauer, D. Jennings, F. Fennessy, M. Sonka, J. Buatti, S. Aylward, J. V. Miller, S. Pieper and R. Kikinis (2012). "3D Slicer as an Image Computing Platform for the Quantitative Imaging Network." Magnetic Resonance Imaging **30**(9): 1323-1341.

Fillinger, M. F., S. P. Marra, M. L. Raghavan and F. E. Kennedy (2003). "Prediction of Rupture Risk in Abdominal Aortic Aneurysm during Observation: Wall Stress versus Diameter." Journal of Vascular Surgery **37**(4): 724-732.

Fillinger, M. F., M. L. Raghavan, S. P. Marra, J. L. Cronenwett and F. E. Kennedy (2002). "In vivo Analysis of Mechanical Wall Stress and Abdominal Aortic Aneurysm Rupture Risk." Journal of Vascular Surgery **36**(3): 589-597.

Fung, Y. C. (1991). "What are the Residual Stresses Doing in Our Blood Vessels?" Annals of Biomedical Engineering, **19**(3): 237-249.

Garlapati, R., A. Roy, G. Joldes, A. Wittek, A. Mostayed, B. Doyle, S. Warfield, R. Kikinis, N. Knuckey, S. Bunt and K. Miller (2014). "More Accurate Neuronavigation Data Provided by Biomechanical Modeling Instead of Rigid Registration: Technical Note." Journal of Neurosurgery **120**.

Garlapati, R. R., A. Mostayed, G. R. Joldes, A. Wittek, B. Doyle and K. Miller (2015). "Towards Measuring Neuroimage Misalignment." Computers in Biology and Medicine **64**: 12-23.

Garlapati, R. R., A. Mostayed, G. R. Joldes, A. Wittek, B. Doyle and K. Miller (2015). "Towards measuring neuroimage misalignment." Computers in Biology and Medicine **64**: 12-23.

Gasser, T. C. (2016). "Biomechanical Rupture Risk Assessment: A Consistent and Objective Decision-Making Tool for Abdominal Aortic Aneurysm Patients." Aorta (Stamford) **4**(2): 42-60.

Gasser, T. C., M. Auer, F. Labruto, J. Swedenborg and J. Roy (2010). "Biomechanical Rupture Risk Assessment of Abdominal Aortic Aneurysms: Model Complexity versus Predictability of Finite Element Simulations." European Journal of Vascular and Endovascular Surgery **40**(2): 176-185.

Gasser, T. C., C. Miller, S. Polzer and J. Roy (2022). "A Quarter of a Century Biomechanical Rupture Risk Assessment of Abdominal Aortic Aneurysms. Achievements, Clinical Relevance, and Ongoing Developments." International Journal for Numerical Methods in Biomedical Engineering **n/a**(n/a): e3587.

Geuzaine, C. and J.-F. Remacle (2009). "Gmsh: A 3-D Finite Element Mesh Generator with Built-in Pre- and Post-processing Facilities." International Journal for Numerical Methods in Engineering **79**(11): 1309-1331.

Geuzaine, C. and J. F. Remacle. (2024). "Gmsh: A three-dimensional finite element mesh generator with built-in pre- and post-processing facilities." from <https://gmsh.info/>.

Hodge, T., J. C. Y. Tan, P. H. Koh, E. Storer, A. Huynh, F. Alkhatib, K. Miller and A. Wittek (2023). Effect of Analyst Segmentation Variability on Computed AAA Stress Distributions Computational Biomechanics for Medicine - Towards Automation and Robustness of Computations in the Clinic. M. P. Nash, A. Wittek, P. M. F. Nielsen et al. Singapore, Springer International Publishing.

Inzoli, F., F. Boschetti, M. Zappa, T. Longo and R. Fumero (1993). "Biomechanical Factors in Abdominal Aortic Aneurysm Rupture." European Journal of Vascular Surgery **7**(6): 667-674.

Joldes, G. R., K. Miller, A. Wittek and B. Doyle (2016). "A simple, effective and clinically applicable method to compute abdominal aortic aneurysm wall stress." Journal of the mechanical behavior of biomedical materials **58**: 139-148.

Joldes, G. R., K. Miller, A. Wittek, R. O. Forsythe, D. E. Newby and B. J. Doyle (2017). "BioPARR: A Software System for Estimating The Rupture Potential Index for Abdominal Aortic Aneurysms." Scientific Reports **7**(1): 4641.

Joldes, G. R., C. Noble, S. Polzer, Z. A. Taylor, A. Wittek and K. Miller (2018). "A Simple Method of Incorporating the Effect of the Uniform Stress Hypothesis in Arterial Wall Stress Computations." Acta of Bioengineering and Biomechanics **20**(3): 59-67.

Joldes, G. R., C. Noble, S. Polzer, Z. A. Taylor, A. Wittek and K. Miller (2018). "A simple method of incorporating the effect of the Uniform Stress Hypothesis in arterial wall stress computations." Acta of Bioengineering and Biomechanics **20**(3): DOI: 10.5277/ABB-01143-02018-01103.

Khosla, S., D. R. Morris, J. V. Moxon, P. J. Walker, T. C. Gasser and J. Golledge (2014). "Meta-analysis of Peak Wall Stress In Ruptured, Symptomatic and Intact Abdominal Aortic Aneurysms." British Journal of Surgery **101**(11): 1350-1357.

Lareyre, F., C. Adam, M. Carrier, C. Dommerc, C. Mialhe and J. Raffort (2019). "A Fully Automated Pipeline for Mining Abdominal Aortic Aneurysm using Image Segmentation." Scientific Reports **9**(1): 13750.

Lesage, D., E. D. Angelini, I. Bloch and G. Funka-Lea (2009). "A Review of 3D Vessel Lumen Segmentation Techniques: Models, Features and Extraction Schemes." Medical Image Analysis **13**(6): 819-845.

Li, M., K. Miller, G. R. Joldes, B. Doyle, R. R. Garlapati, R. Kikinis and A. Wittek (2015). "Patient-specific biomechanical model as whole-body CT image registration tool." Medical Image Analysis **22**(1): 22-34.

Liddel, M., F. Alkhatib, A. Wittek and K. Miller (2023). The Effects of the Spine on the Analysis of Peak Wall Stress in Abdominal Aortic Aneurysms. Computational Biomechanics for Medicine - Towards Automation and Robustness of Computations in the Clinic. M. P. Nash, A. Wittek, P. M. F. Nielsen et al. Singapore, Springer International Publishing.

Liu, M., L. Liang, H. Liu, M. Zhang, C. Martin and W. Sun (2019). "On the Computation of in vivo Transmural Mean Stress of Patient-specific Aortic Wall." Biomech Model Mechanobiol **18**(2): 387-398.

López-Linares, K., N. Aranjuelo, L. Kabongo, G. Maclair, N. Lete, M. Ceresa, A. García-Familiar, I. Macía and M. A. González Ballester (2018). "Fully Automatic Detection and Segmentation of Abdominal Aortic Thrombus in Post-operative CTA images using Deep Convolutional Neural Networks." Medical Image Analysis **46**: 202-214.

Lu, J., X. Zhou and M. L. Raghavan (2007). "Inverse Elastostatic Stress Analysis in Pre-deformed Biological Structures: Demonstration using Abdominal Aortic Aneurysms." Journal of Biomechanics **40**(3): 693-696.

Maier, A., M. W. Gee, C. Reeps, J. Pongratz, H. H. Eckstein and W. A. Wall (2010). "A Comparison of Diameter, Wall Stress, and Rupture Potential Index for Abdominal Aortic Aneurysm Rupture Risk Prediction." Annals of Biomedical Engineering **38**(10): 3124-3134.

Miller, K., H. Mufly, A. Catlin, C. Rogers, B. Saunders, R. Sciarrone, I. Fourneau, B. Meuris, A. Tavner, G. R. Joldes and A. Wittek (2020). "Is There a Relationship Between Stress in Walls of Abdominal Aortic Aneurysm and Symptoms?" Journal of Surgical Research **252**: 37-46.

NICE (National Institute for Health and Care Excellence). (2020). "Abdominal Aortic Aneurysm: Diagnosis and Management (NG156)." from [www.nice.org.uk/guidance/ng156](http://www.nice.org.uk/guidance/ng156)

Rucklidge, W. (1996). The Hausdorff Distance. Efficient Visual Recognition Using the Hausdorff Distance. W. Rucklidge. Berlin, Heidelberg, Springer Berlin Heidelberg: 27-42.

Simulia. (2024). "Abaqus: Finite Element Analysis for Mechanical Engineering and Civil Engineering." from <https://www.3ds.com/products/simulia/abaqus>.

Siriapisith, T., W. Kusakunniran and P. Haddawy (2018). "Outer Wall Segmentation of Abdominal Aortic Aneurysm by Variable Neighborhood Search Through Intensity and Gradient Spaces." Journal of Digital Imaging **31**(4): 490-504.

Speelman, L., E. M. H. Bosboom, G. W. H. Schurink, F. A. M. V. I. Hellenthal, J. Buth, M. Breeuwer, M. J. Jacobs and F. N. van de Vosse (2008). "Patient-Specific AAA Wall Stress Analysis: 99-Percentile Versus Peak Stress." European Journal of Vascular and Endovascular Surgery **36**(6): 668-676.

Vande Geest, J., E. Di Martino, A. Bohra, M. S. Makaroun and D. A. Vorp (2006). "A Biomechanics-Based Rupture Potential Index for Abdominal Aortic Aneurysm Risk Assessment: Demonstrative Application." Annals of the New York Academy of Sciences **1085**: 11-21.

Vorp, D. A., W. A. Mandarino, M. W. Webster and J. Gorcsan (1996). "Potential Influence of Intraluminal Thrombus on Abdominal Aortic Aneurysm as Assessed by a New Non-invasive Method." Cardiovascular Surgery **4**(6): 732-739.

Wanhainen, A., F. Verzini, I. Van Herzelee, E. Allaire, M. Bown, T. Cohnert, F. Dick, J. van Herwaarden, C. Karkos, M. Koelemay, T. Kölbel, I. Loftus, K. Mani, G. Melissano, J. Powell, Z. Szeberin, E. G. Committee, G. J. de Borst, N. Chakfe, S. Debus, R. Hinchliffe, S. Kakkos, I. Koncar, P. Kolh, J. S. Lindholt, M. de Vega, F. Vermassen, r. Document, M. Björck, S. Cheng, R. Dalman, L. Davidovic, K. Donas, J. Earnshaw, H.-H. Eckstein, J. Gollidge, S. Haulon, T. Mastracci, R. Naylor, J.-B. Ricco and H. Verhagen (2019). "Editor's Choice – European Society for Vascular Surgery (ESVS) 2019 Clinical Practice Guidelines on the Management of Abdominal Aorto-iliac Artery Aneurysms." European Journal of Vascular and Endovascular Surgery **57**(1): 8-93.

Wittek, A., F. Alkhatib, R. Vitásek, S. Polzer and K. Miller (2022). "On Stress In Abdominal Aortic Aneurysm: Linear versus Non-linear Analysis and Aneurysm Rupture Risk." International Journal for Numerical Methods in Biomedical Engineering **38**(2): e3554.

Zelaya, J. E., S. Goenezen, P. T. Dargon, A.-F. Azarbal and S. Rugonyi (2014). "Improving the Efficiency of Abdominal Aortic Aneurysm Wall Stress Computations." PLoS One **9**(7): e101353.

Zhu, L., I. Kolesov, Y. Gao, R. Kikinis and A. Tannenbaum (2014). An Effective Interactive Medical Image Segmentation Method using Fast GrowCut. International Conference on Medical Image Computing and Computer-Assisted Intervention. Workshop on Interactive Methods.